Check for updates

# Highly sensitive naphthalimide based Schiff base for the fluorimetric detection of $Fe^{3+}$†

Dhanapal Jothi,[a] Sathishkumar Munusamy,[b] Sathish Sawminathan[a] and Sathiyanarayanan Kulathu Iyer 🟢 *[a]

A simple 1,8-naphthalimide based Schiff base probe (E)-6-((4-(diethylamino)-2-hydroxybenzylidene)amino)-2-(2-morpholinoethyl)-1H-benzo[de]isoquinoline-1,3(2H)-dione (NDSM) has been designed and synthesized for the specific detection of $Fe^{3+}$ based on a fluorimetric mode. The absorbance of NDSM at 360 nm increased significantly in acetonitrile : water (7 : 3, v/v) medium only in the presence of $Fe^{3+}$ ions with a visible colour change from yellow to golden yellow. Likewise, fluorescence emission intensity at 531 nm was almost wholly quenched in the presence of $Fe^{3+}$. However, other competitive ions influenced insignificantly or did not affect the optical properties of NDSM. Lysosome targetability was expected from NDSM due to the installation of a basic morpholine unit. The LOD was found to be 0.8 µM with a response time of seconds. The fluorescence reversibility of NDSM + $Fe^{3+}$ was established with complexing agent EDTA. $Fe^{3+}$ influences the optical properties of NDSM by complexing with it, which blocks C=N isomerization in addition to the ICT mechanism. The real-time application of $Fe^{3+}$ was demonstrated in test paper-based detection, by the construction of a molecular logic gate, quantification of $Fe^{3+}$ in water samples and fluorescence imaging of $Fe^{3+}$.

## Introduction

The intrinsic properties of transition metal ions play an inevitable role in biology and the environment.[1–3] As the most basic and abundant metallic element in the biological system, $Fe^{3+}$ plays a substantial role as an oxygen carrier and aids in the process of electron transfer for the synthesis of ribonucleic acid (RNA) and deoxyribonucleic acid (DNA). In contrast, chronically elevated levels of $Fe^{3+}$ have been associated with fatal diseases including, but not limited to hepatitis, hemochromatosis, various cancers, and possible dysfunction of vital organs, such as the liver, heart, and pancreas.[4–6] Therefore, it is pertinent to develop a highly sensitive and selective probe for the detection of $Fe^{3+}$ ions, which could be pivotal for the early diagnosis of diseases.

Recently optical detection of analytes, especially cations, has attracted significant attention of researchers due to the confluence of advantages such as low detection limit, simplicity of the analytical procedure, high sensitivity and selectivity, and possible naked-eye detection.[7–24] In particular, an arduous effort has been dedicated to manoeuvring fluorescent probes to detect vital analytes. With hindsight, several fluorescent probes have been developed and studied for the detection of $Fe^{3+}$ ion.[25–38] Among them, Schiff bases are generally used motifs.[39–44] In general, Schiff base fluorophores exhibit excited state intramolecular charge transfer (ESIPT) process. ESIPT probes are known for their environment-sensitive emission properties and massive Stokes shift. Coordination with metal ions will inhibit the ESIPT process, and the emission from the keto (K*) tautomer will disappear or get shifted to lower wavelengths. Meanwhile, the stabilized enol form (E*) would show substantial excitation peak.[45–53] Patil et al. have developed a colorimetric probe based on 2-aminoquinolin-3-yl phenyl hydrazone Schiff base for $Fe^{3+}$ chemosensor.[54] Recently, a new Schiff-based macrocyclic host has been reported for the sensing and removal of $Fe^{3+}$.[55] Finelli et al. reported salen-type anthracene-based probe for the selective fluoro-colourimetric detection of $Fe^{3+}$.[56] Phenol-based Schiff base, 4-pyridine-2-ylmethyleneaminophenol (PYAP) was found to be highly sensitive towards $Fe^{3+}$ low-level detection with the naked eye.[57,58] Most of these ligands suffer from low sensitivity, irreversible sensing and poor subcellular selectivity.

The photophysical properties and diagnostic application of 4-aminonaphthalimide scaffolds have been ardently studied.[59–61] The integral property of photostability and unhindered cell permeability makes 4-aminonaphthalimide derivative an immediate candidate for fluorescence bioimaging. Furthermore, these compounds display a fervent intramolecular charge (ICT) transfer from electron-donating amine

[a]Department of Chemistry, School of Advanced Sciences and Vellore Institute of Technology, Vellore-632014, India. E-mail: sathiya_kuna@hotmail.com

[b]Institute of Chemical Biology and Nanomedicine, State Key Laboratory of Chemo/Biosensing and Chemometrics, College of Chemistry and Chemical Engineering, Hunan University, Changsha 410082, P. R. China. E-mail: pra3sat@gmail.com

to imide. Due to ICT, most of these compounds are sensitive to the polarity of the solvent medium. Besides, the spectroscopic and binding profile of these compounds can be fine-tuned by incorporating an appropriate functional group on C-4 position. Further, the imide group can be installed with subcellular targetable moiety. As garbage disposing cellular organelle, liposomes host iron storing macromolecules, ferritin and electron transport proteins which enhance the accumulation of iron in liposomes.[62,63] With these compounding facts, we envisage that lysosome specific sensitive and selective fluorescent detection of $Fe^{3+}$ will be an immense stride towards the understanding of $Fe^{3+}$ metabolism.

With these insights in view, herein, we report naphthalimide – Schiff based hybrid fluorescence 'On–Off–On' type fluorescent probe **NDSM**. This can act as a fluorometric/colorimetric detection probe for $Fe^{3+}$ with high selectivity and sensitivity. The obtained experimental results revealed **NDSM** with a remarkable low limit of detection (LOD), anti-interference from other metal ions, reasonably quick response and reversibility of the fluorescence. The fluorescence quenching commenced from the complexation between **NDSM** and $Fe^{3+}$. The complexed $Fe^{3+}$ can be successfully retrieved using EDTA. Real-time analysis in various water bodies revealed that **NDSM** could be successfully implemented in pollution inspection of $Fe^{3+}$ and bioimaging studies, which confirmed **NDSM** as a vital imaging probe for $Fe^{3+}$.

# Experimental section

All common reagents and solvents were purchased as AR grade from commercial sources, blood sample to prepare deproteinized human serum was received from health center of Vellore Institute of Technology, Vellore campus. *E. coli* strains were purchased from Sigma Aldrich. $^{1}H$ and $^{13}C$ NMR spectra of compounds were recorded using Bruker 400 MHz instrument. UV-visible absorption spectra were taken using a Hitachi U-2910 spectrophotometer. Fluorescence spectra were recorded using a Hitachi F-7000 fluorescence spectrometer. Biological images were recorded on WEXWOX fluorescence research microscope 3000. Quantum yields were calculated using quinine sulfate ($\Phi_{fl}$ = 0.54 in 0.5 M $H_2SO_4$ solution) as a reference standard. FTIR spectrum was performed on a Jasco-4100 instrument. LC-MS was recorded using Agilent 6495 LCMSMS instrument.

## Synthesis of compound-1

4-Bromo-1,8 naphthalic anhydride (1 g, 0.003 mmol) and 2-morpholinoethan-1-amine (0.564 g, 0.004 mmol) were dissolved in 25 mL of anhydrous ethanol solvent. This reaction mixture was refluxed for 10 h and the completion of the reaction was monitored by TLC. After the completion of the reaction, the reaction mixture was allowed to cool to room temperature, filtered and washed with diethylether to give pure yellow color solid. Yield 80%; $^{1}H$ NMR (400 MHz, DMSO-$d_6$): $\delta$ 2.5834–2.595 (t, 4H, 2× $CH_2$, $J$ = 4.64 Hz), 2.685–2.702 (t, 2H, $CH_2$, $J$ = 6.8 Hz), 3.665–3.676 (t, 4H, 2× $CH_2$, $J$ = 4.4 Hz), 4.307–4.324 (t, 2H, $CH_2$, $J$ = 6.8 Hz), 7798–7.810 (t, 1H, ArCH, $J$ = 4.8), 7.984–7.994 (t, 1H,

ArCH, $J$ = 4 Hz), 8.340–8.351 (t, 1H, ArCH, $J$ = 4.4 Hz), 8.503–8.524 (d, 1H, ArCH, $J$ = 8.4 Hz), 8.591–8.599 (d, 1H, ArCH, $J$ = 3.2 Hz). $^{13}C$ NMR (DMSO-$d_6$, 100 MHz): $\delta$ 37.32, 53.81, 56.08, 67.03, 122.11, 122.98, 128.92, 130.27, 130.54, 131.07, 131.17, 131.99, 133.23, 163.51, 163.54.

## Synthesis of compound-2

Compound-**1** (500 mg, 0.00128 mmol) and sodium azide (215 mg, 0.00385 mmol) were mixed in 20 mL of HPLC-DMSO solvent medium under nitrogen atmosphere. The reaction mixture was allowed to react at 100 °C for 5 hours. After the completion of the reaction, the reaction mixture was allowed to cool at room temperature, and NaSH (271 mg, 0.0032 mmol) was added. The mixture was vigorously stirred for about 3 hours. After the completion of the reaction (monitored on TLC), cold water was added to the reaction mixture and the resulting yellow color precipitate was filtered and washed with 10 mL of diethyl ether and dried. Yield 90%; $^{1}H$ NMR (400 MHz, DMSO-$d_6$): $\delta$ 2.451–2.507 (t, 6H, 3× $CH_2$, $J$ = 22.4 Hz), 3.5254–3.5349 (t, 4H, 2× $CH_2$, $J$ = 3.8 Hz), 4.117–4.134 (t, 2H, $CH_2$, $J$ = 6.8 Hz), 6.827–6.848 (d, 1H, ArCH, $J$ = 8.4 Hz), 7.450 (s, 2H, $NH_2$), 7.622–7.641 (t, 1H, ArCH, $J$ = 7.6 Hz), 8.169–8.190 (d, 1H, ArCH, $J$ = 8.4 Hz), 8.402–8.420 (d, 1H, ArCH, $J$ = 7.2 Hz), 8.595–8.616 (d, 1H, ArCH, $J$ = 8.4 Hz). $^{13}C$ NMR (DMSO-$d_6$, 100 MHz): $\delta$ 36.82, 53.89, 56.28, 66.68, 107.94, 108.62, 119.81, 122.19, 124.43, 129.78, 130.16, 131.47, 134.43, 153.20, 163.32, 164.23.

## Synthesis of NDSM

To a suspension of compound **2** (500 mg, 0.0015 mmol), 4-(diethylamino) salicylaldehyde (356 mg, 0.0018 mmol) was added in absolute ethanol (20 mL) and catalytic amount of acetic acid (18 μL, 0.003 mmol) was added to the same solution. The resulting solution was stirred at 90 °C for 10 hours. After cooling it to room temperature, the reaction mixture was monitored by TLC and the crude product was purified by column chromatography using *n*-hexane/ethylacetate (1 : 1) as an eluent to afford compound **NDSM** as an orange solid with 82% yield; $^{1}H$ NMR (400 MHz, DMSO-$d_6$): $\delta$ 1.1174 (t, 3H, $CH_3$), 2.2870–2.5078 (d, 5H, $CH_2$, $J$ = 3.8 Hz), 3.1758–3.3947 (m, 10H, $CH_2$, $J$ = 6.8 Hz), 4.0120–4.0364 (d, 2H, $CH_2$, $J$ = 8.4 Hz), 4.3752 (s, 2H, $CH_2$), 6.0492 (s, 1H, ArCH, $J$ = 7.6 Hz), 6.3346–6.3532 (d, 1H, ArCH, $J$ = 8.4 Hz), 6.8743–6.8916 (d, 1H, ArCH, $J$ = 7.2 Hz), 7.1034–7.1170 (d, 1H, ArCH, $J$ = 8.4 Hz), 7.4124–7.4331 (d, 1H, ArCH, $J$ = 8.4 Hz), 8.2167–8.2341 (d, 1H, ArCH, $J$ = 8.4 Hz), 8.4555–8.467 (d, 1H, ArCH, $J$ = 8.4 Hz), 8.6669–8.6847 (d, 1H, ArCH, $J$ = 8.4 Hz), 9.6176 (s, 1H, C=N), 11.2487 (s, 1H, OH). $^{13}C$ NMR (DMSO-$d_6$, 100 MHz): $\delta$ 12.90, 34.35, 44.58, 52.07, 54.84, 63.77, 96.41, 104.94, 111.70, 119.82, 122.15, 124.50, 125.95, 128.51, 130.19, 131.75, 134.43, 134.74, 138.06, 146.19, 163.73, 163.86, 164.85. HRMS for $C_{29}H_{32}N_4O_4$. Calculated [M$^+$] $m/z$ 501.2424, found: 501.2480.

## UV-visible absorption and fluorescence studies

The UV-visible absorption and fluorescence studies of the probe **NDSM** were carried out using 2 × 10$^{-5}$ M solution. A stock solution of probe **NDSM** (2 × 10$^{-3}$ M) was prepared in $CH_3CN$.

Metal stock solution ($1 \times 10^{-3}$ M) was prepared by adding various metal salts in double-distilled water. Absorption spectra were recorded using 1 cm quartz cell, and the range of spectra recorded was 200–800 nm. The emission spectra were obtained using quartz cuvette of 10 mm, 5 nm slit width, and performed by excitation at 344 nm, medium sensitivity and 1 second response time.

Fluorescence and absorption measurements were performed as follows: appropriate volume from a stock solution of metal ions ($1 \times 10^{-3}$ M, $H_2O$) was added to the 2 mL of **NDSM** ($2 \times 10^{-5}$ M, $CH_3CN : H_2O$ (7 : 3)) solution. For determination of $Fe^{3+}$ in the human serum sample, deproteinized human serum sample was prepared according to the literature procedure. Aliquots of the above deproteinized human serum sample were added to 2 mL of **NDSM** solution, and the emission spectra were recorded immediately.

### Equations

The binding constant ($K_b$) was calculated from fluorescence titration using modified Benesi–Hildebrand (B–H) equation (eqn (1)). The value of intercept and slope were taken from the plot of $1/[F − F_0]$ versus $1/[Fe^{3+}]$.

$$1/(F − F_0) = 1/K_b \times 1/(F_{max} − F_0) \times 1/[Fe^{3+}] + 1/(F_{max} − F_0) \quad (1)$$

In this equation, $F_0$ represents initial fluorescence intensity, $F$ stands for fluorescence intensity of **NDSM** in the presence of a given concentration of $Fe^{3+}$, $F_{max}$ represents the saturated intensity of probe **NDSM** in the presence of the excess amount of $Fe^{3+}$ and $K_b$ represents a binding constant.

For the calculation of limit of detection (LOD), $3\sigma$ method was followed as given in the following equation.

$$LOD = 3\sigma/K \quad (2)$$

In this equation, $\sigma$ stands for standard deviation calculated from six independent blank measurements, and $K$ is the slope calculated from the Stern–Volmer plot (eqn (3)).

$$F_0/F = 1 + K_{SV}[Q] \quad (3)$$

Here, $K_{SV}$ stands for Stern–Volmer quenching constant.

Equation followed to calculate quantum yield is as follows (eqn (4)).

$$\phi\_x = \phi\_s \times F\_u/F\_s \times A\_S/A\_u \quad (4)$$

where $\Phi$ is the quantum yield, $F$ is an integrated area of corresponding fluorescence and $A$ stands of the corresponding absorbance.

### Preparation of test paper

Test paper strips were immersed in the probe solution of **NDSM** (20 μM in $CH_3CN$) and then dried well in a hot air oven at 40 °C for 30 minutes. These test paper strips were tested with the addition of aqueous solution (1 mM) of various sensing metal ions and were irradiated under UV light of 365 nm. Additionally,

the sensor probe **NDSM** test strips were studied with the solution of $Fe^{3+}$ (aqueous medium) with different concentrations varying from 0 to 5 equivalents.

### Bioimaging of NDSM in *E. coli* cells

Freshly prepared *E-coli* cells grown in Luria–Bertani medium were used for bioimaging analysis. The stock solution (20 μM) was prepared by dissolving **NDSM** in 70% acetonitrile in water (v/v). The prepared cells were washed with phosphate-buffered saline (PBS) and incubated with **NDSM** at 37 °C for 30 min. After incubation, fluorescence images of *E. coli* cells were recorded using WEXWOX fluorescence research microscope. Blue channel of the range between 400–500 nm was used. Then, *E. coli* cells treated with **NDSM** were added with $Fe^{3+}$ solution and incubated for 30 min at 37 °C, and washed thrice with PBS buffer. Finally, the cells were imaged on a fluorescence microscope.

## Results and discussion

### Design and synthesis of probe NDSM

The synthesis of **NDSM** was attained in good yields, as depicted in Scheme S1,† and the structure is given in Scheme S1 (see ESI file Scheme S1†). The structure and the purity of product **NDSM** were confirmed by $^1H$, $^{13}C$ NMR, and LC-MS analysis (Fig. S1–S3†). As can be seen in the Scheme S1 (see ESI file Scheme S1†), lysosome targeting morpholine moiety is installed on naphthalimide as an amide. Compound **NDSM** was allowed to react with 4-(diethylamino)-2-hydroxybenzaldehyde to form a Schiff base which is the binding unit for $Fe^{3+}$. Bright emission from **NDSM** emanates from ICT. Complexation of $Fe^{3+}$ with **NDSM** blocking of ICT to quench the fluorescence of **NDSM**. Additionally, widely known complexing agent EDTA can retrieve $Fe^{3+}$ from **NDSM–Fe³⁺** complex to recuperate the fluorescence of **NDSM**.

### Spectroscopic property and optical responses to Fe³⁺

The absorption spectrum of **NDSM** ($2 \times 10^{-5}$ M) in acetonitrile : water (7 : 3) solvent showed weak absorption peak at 344 nm (7500 $mol^{-1}$ $dm^3$ $cm^{-1}$) and 430 nm (2500 $mol^{-1}$ $dm^3$ $cm^{-1}$) (Fig. S4†). To begin with, the absorption spectrum of **NDSM** was recorded with 10 equivalents of various metal ions. As can be seen in Fig. 1, of the various metals added, only $Fe^{3+}$ instilled a distinguishable change in the absorption spectrum of **NDSM**. Addition of only two equivalents of $Fe^{3+}$ brought about a new and clear peak at around 360 nm (105 500 $mol^{-1}$ $dm^3$ $cm^{-1}$). Other metal ions had very little or no effect on the absorption of **NDSM**.

Furthermore, the addition of $Fe^{3+}$ caused a phenomenal 30-fold increase in the molar absorptivity. Metal to ligand charge transfer can be ascribed to the enhancement of absorption at 360 nm. In free **NDSM**, isomerization at C=N weakened the ligand-to-ligand charge transfer which in turn led to feeble ICT absorption band. Selective complexation with $Fe^{3+}$ hindered isomerization at C=N, which led to strong ICT transition and absorption. This result implies the selective sensing of **NDSM**
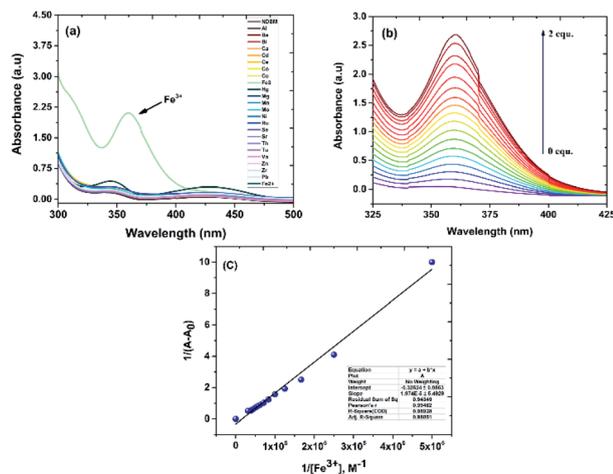
Fig. 1 (a) UV-vis spectra of NDSM ($2 \times 10^{-5}$ M) in the absence and presence of various metal ions. (b) UV-vis spectra of NDSM ($2 \times 10^{-5}$ M) in acetonitrile/water (7 : 3) mixture with the incremental addition of (0–2 equiv.) of $Fe^{3+}$. (c) B–H nonlinear curve fitting plot (absorbance at 360 nm) of probe NDSM assuming 1 : 1 binding stoichiometry with $Fe^{3+}$.



Fig. 2 (a) Selectivity and anti-interference of NDSM in ACN : water (7 : 3) medium in the presence of $Fe^{3+}$ (2 equiv.) and miscellaneous cations (10 equiv.) at 531 nm. (b) Change in fluorescence intensity of NDSM over the incremental addition of $Fe^{3+}$. Inset: Stern–Volmer plot. (c) Photographs of NDSM in the presence of various metals and $Fe^{3+}$ under a UV lamp at 365 nm.

towards $Fe^{3+}$. The quantitative sensing of $Fe^{3+}$ by NDSM was analyzed by the incremental addition of $Fe^{3+}$ leading to saturation during the addition of 2 equivalents (Fig. 1b). The ligand absorption at 360 nm underwent gradual and remarkable enhancement with a bathochromic shift, substantiating the complexation and restrained C=N isomerization. According to Benesi–Hildebrand (B–H plot) nonlinear curve fitting method, plot between absorption intensity ratio and 1/[$Fe^{3+}$] was plotted, which confirmed 1 : 1 binding stoichiometry of NDSM and $Fe^{3+}$ (Fig. 1c). From this plot, the association constant was found to be $K_a = 1.68 \times 10^4$ $M^{-1}$ for the NDSM + $Fe^{3+}$ complex.

### Fluorescence studies on the detection of $Fe^{3+}$ by NDSM

Encouraged by UV-vis studies, we extended sensing study of NDSM to fluorescence platform. Probe NDSM ($2 \times 10^{-5}$ M) displayed a strong fluorescence emission at 531 nm when excited at 344 nm UV light with $\Phi_{Fl}$ calculated to be 0.28 (quinine sulfate in 0.1 N $H_2SO_4$ as a standard). The Stokes shift was found to be 53 475 $cm^{-1}$ (187 nm), which is relatively large due to the cooperation of ESIPT and ICT processes in the Schiff base region. The influence of various metal ions on the emission property of NDSM was studied and is displayed in Fig. S5.† Fluorescence of NDSM was almost wholly quenched over the addition of 2 equivalence of $Fe^{3+}$, whereas other metal ions were unable to affect the fluorescence of NDSM. This indicates that probe NDSM can act as a selective "turn-off" sensor for the detection of $Fe^{3+}$.

The interference of other competitive metal ions and anions over the detection of $Fe^{3+}$ using NDSM was studied. As can be seen from Fig. 2a, the sensing was perturbed by the presence of other ions, even 10 equivalents, which indicated high selectivity of NDSM towards $Fe^{3+}$. Besides, bright and clear yellow emission of the probe was completely switched off when viewed under the UV light (Fig. 2c), whereas other metal ions retained
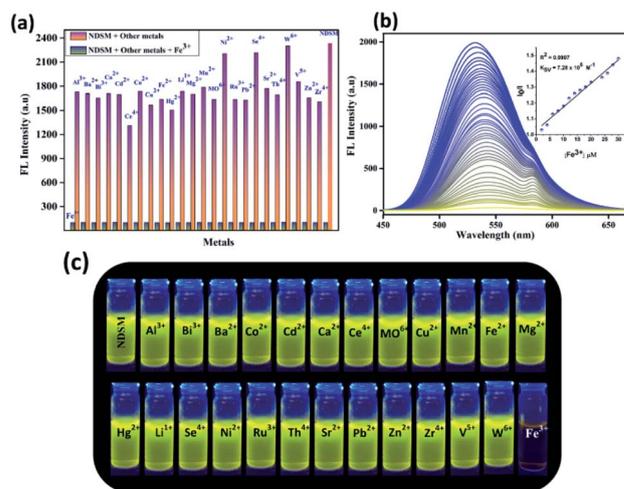
the yellow emission. Using the UV-vis spectra, the quantitative sensing ability of NDSM towards $Fe^{3+}$ was studied by the titration method, as shown in Fig. 2b. The fluorescence intensity changes over the gradual increase of the concentration of $Fe^{3+}$ were investigated. The fluorescence intensity decrease at 531 nm was gradual, with increasing concentration of $Fe^{3+}$, which eventually became constant at two equivalents of $Fe^{3+}$. As can be seen in Fig. 2b (inset), the plot of $I_0/I$ maintains a linear relationship between the concentration of $Fe^{3+}$ and emission intensity of NDSM. Using $3\sigma/K$ method, the detection limit was calculated from emission titration method, which was found to be 0.81 μM (Fig. S6†).

### Electrochemical study

Cyclic voltammetry (CV) experiments were performed with NDSM modified glassy carbon electrode (GCE-NDSM) in an electrolyte with pH 7 phosphate buffer (PBS) solution at a scan rate of 50 mV $s^{-1}$ under a nitrogen atmosphere to determine the electrochemical behaviour as well as charge transfer process. As can be seen from Fig. S7† a feeble redox peak appeared around 0.15 to 0.2 V vs. Ag/AgCl due to the presence of ICT process in the molecule. The estimated HOMO ($E_{HOMO} = E_{LUMO} - E_{gap}$) and LUMO ($E_{LUMO} = -4.8$ eV $- E_{red}$) energy gaps $-7.55$ eV and $-4.95$ eV, respectively were found almost close to the structural motif characteristic of good charge transition. Moreover, for NDSM the energy difference ($\Delta E$) estimated through CV (2.6 eV) and UV-vis absorption (2.52 eV) (Fig. S7b†) methods suggested that probe NDSM is a suitable D–A system with possibility of ICT.

### Effect of pH and time response

The effect of pH on the emission behaviour NDSM and $Fe^{3+}$ at various pH values was studied to comprehending the practical
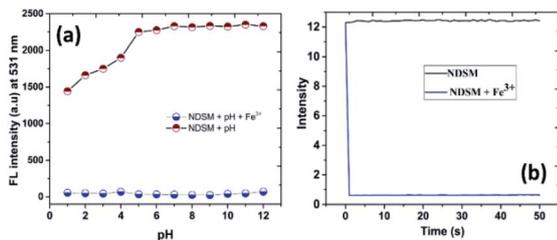
**Fig. 3** (a) Effect of pH on the fluorescence response of NDSM and NDSM + $Fe^{3+}$. (b) Fluorescence response time of NDSM over the addition of $Fe^{3+}$.

utility of probe to detect $Fe^{3+}$ (Fig. 3a). Experimental results demonstrated that the fluorescence of free **NDSM** was not affected in pH window of 5–12. This suggests that the probe has not been affected in this pH range. But when the pH of the medium was reduced further, a significant decline in emission intensity was observed, and the lowest emission intensity was recorded at pH = 1. This could be due to the interference of ESIPT in strongly acidic condition. However, the quenched fluorescence of **NDSM** + $Fe^{3+}$ was not affected in the entire pH region tested. Thus, detection of $Fe^{3+}$ using **NDSM** can be realized in the pH range of 5–12, especially under the physiological and neutral pH conditions. Besides, the fluorescence response time of **NDSM** towards the addition of $Fe^{3+}$ was studied by monitoring fluorescence *vs.* time. As shown in Fig. 3b, the addition of $Fe^{3+}$ to **NDSM** caused immediate quenching of emission and reached the plateau in 2 seconds. This demonstrates there is an instant complex formation between **NDSM** and $Fe^{3+}$. This indicates cultivation time free detection of $Fe^{3+}$ by **NDSM** with potential applicability in real-time applications.

### Binding stoichiometry and sensing mechanism

To get an insight into the complexing stoichiometry between **NDSM** and $Fe^{3+}$, B–H a linear curve was plotted, as shown in Fig. 4a. The linear tendency of the B–H plot indicates there is 1 : 1 complex formation between **NDSM** and $Fe^{3+}$. From this linear plot, the association binding constant ($K_a$) was calculated to be $2.49 \times 10^4$ $M^{-1}$. Additionally, Job's plot method was used to evaluate the binding stoichiometry between **NDSM** and $Fe^{3+}$.

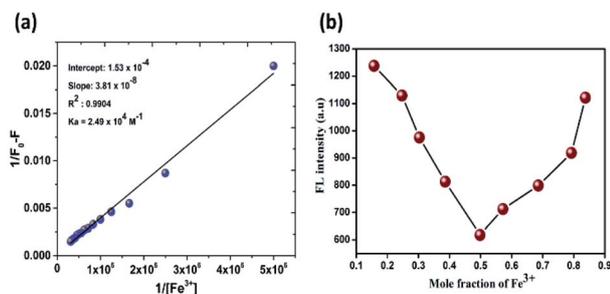As can be seen in Fig. 4b, the fluorescence intensity of **NDSM** + $Fe^{3+}$ was plotted against molar fraction by maintaining constant total concentration. The deflection point appeared at 0.5 molar ratio, which indicates 1 : 1 binding mode between **NDSM** and $Fe^{3+}$.

The binding event of the **NDSM** with $Fe^{3+}$ is represented in Fig. S8.† The complexation of $Fe^{3+}$ on the Schiff base region of the probe is responsible for the concomitant optical event of the probe. FT-IR and LC-MS experiments were carried out to further confirm the binding mechanism. In FT-IR (Fig. S9†), the characteristic phenolic O–H stretching frequency of **NDSM** that appeared at 3441 $cm^{-1}$ got broadened and shifted to 3539 $cm^{-1}$. The stretching vibration of the imine C=N group of ligand at 1581 $cm^{-1}$ completely disappeared in the complex system. This indicates $Fe^{3+}$ forms complex with **NDSM** by interaction with the nitrogen atom of imine and phenolic –OH. LC-MS analysis of **NDSM**–$Fe^{3+}$ showed exact mass value for the formed 1 : 1 complex (Fig. S10†).

### Reversibility study

For real-time application and from the economic aspect, reversibility is the vital parameter of the probe. To validate the reversibility of **NDSM** sensor towards $Fe^{3+}$, a fervent complexing agent EDTA was added to the solution of **NDSM**–$Fe^{3+}$ complex system. Initially, free **NDSM** exhibits intense fluorescence and addition of $Fe^{3+}$ quenched the emission almost wholly. To this solution, one equivalent of $Na_2$–EDTA was added, and the emission was recorded immediately. As can be seen in the Fig. 5a, the addition of $Na_2$–EDTA ligand to the mixture of **NDSM** and $Fe^{3+}$ caused almost complete recovery of the lost fluorescence, almost immediately, with previous intensity due to the formation of EDTA + $Fe^{3+}$ complex and subsequent regeneration of the free **NDSM**. This "ON–OFF–ON" switching behavior at 531 nm of **NDSM** towards $Fe^{3+}$ and EDTA can be repeated for about five times with very little loss in the initial emission intensity (Fig. 5b). This experiment suggests excellent reusability of the **NDSM** for the detection of $Fe^{3+}$ *via* the addition of cheap and readily available EDTA ligand.

### Molecular logic gate behavior of NDSM

Inspired by the excellent reversible sensing behavior of **NDSM** towards $Fe^{3+}$ and EDTA, we intended to construct a molecular logic gate. The emission sensitivity changes at 531 nm of **NDSM**
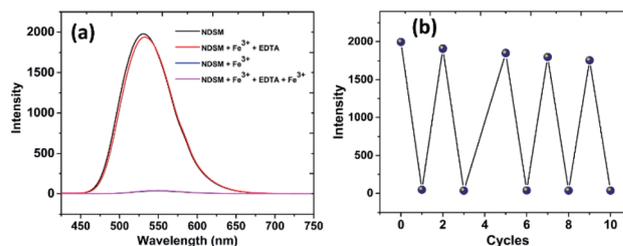


**Fig. 4** (a) B–H plot of the 1 : 1 complex of probe NDSM and $Fe^{3+}$ ions; (b) Job's plot for determining the stoichiometry of NDSM and $Fe^{3+}$ ions.



**Fig. 5** (a) Fluorescence intensity responses of NDSM ($2 \times 10^{-5}$ M) in ACN-$H_2O$ medium (7 : 3 v/v) upon addition of $Fe^{3+}$ + EDTA; (b) number of sequential detections of $Fe^{3+}$ and EDTA.
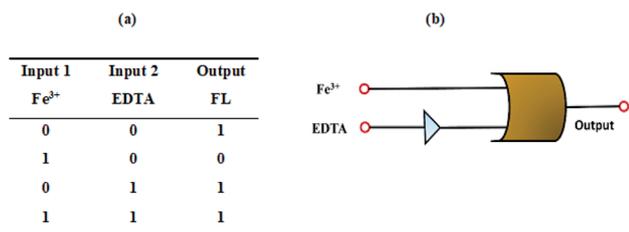
Paper

**Fig. 6** (a) Truth table (1 = on; 0 = off states). (b) Pictorial representation of logic gate with two input, $Fe^{3+}$ and EDTA.
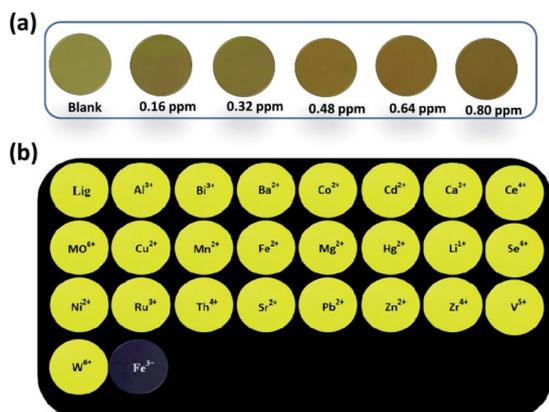


**Fig. 7** (a) Photograph of paper-based strips indicating concentration-dependent change in the color profiles of **NDSM** over the addition of $Fe^{3+}$; (b) the photographic images represent the paper-based strips of **NDSM** with various metal ions under UV illumination (365 nm).

in the presence of guest species ($Fe^{3+}$ and EDTA) was taken as the output to design implication logic gate. The fluorescent probe as such remains in "turned-on" state as such and in the presence of EDTA which was considered as the ON mode (output = 1). While the fluorescence of **NDSM** turned-off entirely in the presence of $Fe^{3+}$, it is regarded as OFF mode (output = 0). Based on this input, four possible input functions can be derived, such as (0, 0), (1, 0), (0, 1) and (1, 1) and the truth table is presented in the Fig. 6a condition (0, 0) is where none of the analytes ($Fe^{3+}$, EDTA) is present, and the output signal is "0".

In the presence of input ($Fe^{3+}$) to **NDSM**, the emission at 531 nm is quenched and leads to the function (1, 0) with output "0" whereas input EDTA leaves **NDSM** "turned-on" and function is represented as (0, 1) with output "1". Finally, the simultaneous existence of both inputs ($Fe^{3+}$ and EDTA), *i.e.* (1, 1), the emission at 531 is restored showing output signal "1". Based on this, a logic gate was constructed, and it is shown in the Fig. 6b. With the IMPLICATION operation of NOT gate and OR gate, this designed logic circuit could convert two inputs ($Fe^{3+}$, EDTA) into the output of **NDSM** fluorescence at 531 nm.

### Detection of $Fe^{3+}$ by NDSM by paper-based array system

With the proven detection performance of **NDSM** in the solution state, the detection potential was also extended to the paper-based sensor. Whatman filter paper was facilely fabricated with **NDSM** by the drop-casting method. The naked eye observation in ambient sunlight indicated a golden yellow color. As can be seen in Fig. 7a, the golden yellow thickened over the instant exposure of $Fe^{3+}$. The test strip became darker in color with the increasing concentration of $Fe^{3+}$ (0.16–0.8 ppm). Notably, the test strips could produce a discernible response at concentration as low as 0.16 ppm. Visual detection was also monitored by exposing the test paper under a UV lamp (Ex = 365 nm). The fluorescence response of the filter paper was monitored by exposing different metal ions. As depicted in Fig. 7b, the bright yellow fluorescence of the paper strip was not affected by metal ions tested except $Fe^{3+}$. Contact with $Fe^{3+}$ has caused immediate quenching of the color in filter paper. Besides, the bright yellow fluorescence gradually faded away over the increasing concentration of $Fe^{3+}$ and emission intensity inversely proportional to the concentration of $Fe^{3+}$. These results demonstrate that **NDSM** can be used as a portable preliminary sensor platform for $Fe^{3+}$.

### Application of NDSM in practical water analysis

To investigate the practical utility of **NDSM**, fluorescence detection of **NDSM** to $Fe^{3+}$ was carried out in water samples collected from different water bodies of Vellore district. The collected water samples were spiked with the known concentrations of $Fe^{3+}$, and their influence on the fluorescence of **NDSM** was analyzed by recording the emission intensity. Three

**Table 1** Estimation of $Fe^{3+}$ ion quantity in collected water samples

| S. No. | Water samples[a] | $Fe^{3+}$ spiked (M) | $Fe^{3+}$ found (M) | Recovery (%) | R.S.D[b] ($n = 3$) (%) |
|---|---|---|---|---|---|
| 1 | Tap water | $2 \times 10^{-5}$ | $1.91 \times 10^{-5}$ | 98.56 | 0.19 |
| 2 | Lake water | $2 \times 10^{-5}$ | $1.95 \times 10^{-5}$ | 98.81 | 0.35 |
| 3 | Well water | $2 \times 10^{-5}$ | $1.93 \times 10^{-5}$ | 97.91 | 0.21 |
| 4 | Mineral water | $2 \times 10^{-5}$ | $1.96 \times 10^{-5}$ | 98.81 | 1.03 |
| 5 | Distilled water | $2 \times 10^{-5}$ | $1.93 \times 10^{-5}$ | 98.46 | 0.28 |
| 6 | Purified water | $2 \times 10^{-5}$ | $1.97 \times 10^{-5}$ | 97.96 | 0.23 |
| 7 | Human serum albumin | $2 \times 10^{-5}$ | $1.89 \times 10^{-5}$ | 94.51 | 0.26 |

[a] Water samples were collected from in and around VIT campus, Vellore. [b] relative standard deviation; conditions: 20.00 μM **NDSM** in mixed solution of $CH_3CN$/river water (7 : 3).
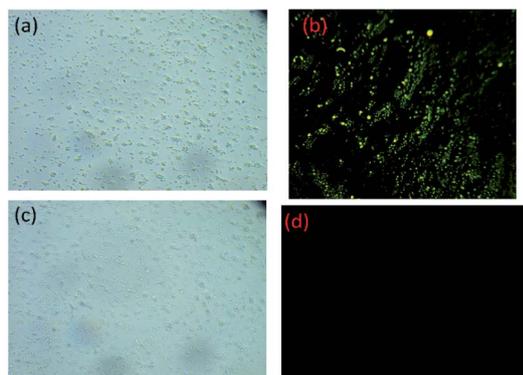
**Fig. 8** Fluorescent cell imaging: (a) bright-field image of *E. coli* cells; (b) fluorescent field image of **NDSM** treated *E. coli* cells; (c) bright-field image of *E. coli* cells; (d) fluorescent field image of **NDSM** treated *E. coli* cells incubated with $Fe^{3+}$ ions.

successive measurements were carried out to detect the mean detection value of $Fe^{3+}$. As can be shown in Table 1, the spiked concentration of $Fe^{3+}$ has been detected with satisfactory recovery and relative stand deviation (R.S.D.). These results indicate **NDSM** can successfully detect with high selectivity and accurate quantification.

### Fluorescent imaging of $Fe^{3+}$ ions in *E-coli* cells

Cytotoxicity of **NDSM** was studied using red blood cells (RBC) by adding different concentrations of **NDSM** to RBC cell culture medium and incubated for about 24 h. The cell viability was found to be more than 95% at the **NDSM** concentration of $2 \times 10^{-5}$ M, which indicates that cells can endure low concentration of **NDSM** for a long period. Hence, **NDSM** can be used for the bioimaging of $Fe^{3+}$ in living cells. Accordingly, *in vitro* fluorescence imaging of $Fe^{3+}$ was carried out by incubating **NDSM** (in DMSO/$H_2O$ (2 : 8 v/v)) with *E. coli* cells buffered with Luria–Bertani medium and the imaging was carried out after 30 minutes. As can be seen in Fig. 8. *E. coli* cells incubated with **NDSM** showed clear and intense yellow color emission when visualized under fluorescence microscopy. Another set of *E. coli* cell incubated with **NDSM** was added and incubated with 10 μM $Fe(NO_3)_3$. Fluorescence imaging of these cells showed a yellow emission of **NDSM**, which was entirely quenched by $Fe^{3+}$. Additionally, the brightfield image of $Fe^{3+}$ treated cells showed the clear and intact appearance of cells which indicates the viability of the cells throughout the imaging experiment. Due to the negligible cytotoxicity, biocompatibility, cell permeability and conspicuous imaging of $Fe^{3+}$, **NDSM** can be used to detect $Fe^{3+}$ in living cells.

## Conclusions

In this work, we designed and synthesized 1,8-naphthalimide based Schiff base probe (**NDSM**) and confirmed its molecular structure by NMR, LC-MS and HRMS analysis. The synthesized probe was able to detect $Fe^{3+}$ in the presence of various other competitive ions in the organic medium. **NDSM**, as such, is

yellow in color and a bright yellow emitting compound. Concerted analysis of both absorption and emission spectra of **NDSM** in the presence $Fe^{3+}$ revealed that **NDSM** could act as an efficient and economical optical probe for the selective detection of $Fe^{3+}$. B–H and Job's plot analysis showed that there was 1 : 1 complexation between **NDSM** and $Fe^{3+}$. Optical response of **NDSM** towards $Fe^{3+}$ was rapid. **NDSM** has very high sensitivity towards $Fe^{3+}$ as evident from the very low LOD values (nanomolar range). IR and LC-MS analyses revealed that $Fe^{3+}$ forms a complex with **NDSM** by coordinating with C=N and –OH functional groups. The optical property of **NDSM** can be regenerated entirely from **NDSM** + $Fe^{3+}$ with the addition of EDTA, and the reversible detection of $Fe^{3+}$ can be realized several times. The potential real-time application of **NDSM** has been successfully demonstrated in various platforms, such as paper-based testing, analysis in different water bodies, molecular logic function and bioimaging analysis in *E. coli*. Therefore, **NDSM** can be used as a potential platform for the chromogenic and fluorogenic detection of $Fe^{3+}$.

## Ethical statement

All the experiments, the results of which have been represented in the manuscript, were performed in compliance with relevant laws or guidelines by ICMR (Govt. of India).

All the experiments, the results of which have been represented in the manuscript, have followed the institutional (VIT) guidelines.

Our application for approval is under the consideration of the Institutional Ethical Committee. A certificate from the Ethical Committee is also appended herewith.

An informed consent, as stipulated by the Institutional Ethical Committee, has been obtained from each of the volunteers before collecting the sample.

## Conflicts of interest

There are no conflicts to declare.

## Acknowledgements

## Notes and references

1 A. M. Brokesh and A. K. Gaharwar, *ACS Appl. Mater. Interfaces*, 2020, **12**, 5319–5344.
2 D. Buccella, M. H. Lim and J. R. Morrow, *Inorg. Chem.*, 2019, **58**, 13505–13508.
3 *Nat. Chem. Biol.*, 2008, **4**, 143.
4 X. Huang, *Mutat. Res.*, 2003, **533**, 153–171.

5  D. Galaris, V. Skiada and A. Barbouti, *Cancer Lett.*, 2008, **266**, 21–29.

6  H. Kozlowski, M. Luczkowski, M. Remelli and D. Valensin, *Coord. Chem. Rev.*, 2012, **256**, 2129–2141.

7  P. Lesani, G. Singh, C. M. Viray, Y. Ramaswamy, D. M. Zhu, P. Kingshott, Z. Lu and H. Zreiqat, *ACS Appl. Mater. Interfaces*, 2020, **12**, 18395–18406.

8  J. Li, L. Yang, Y. Ruan, S. Chu, H. Wang, Z. Li, C. Jiang, B. Liu, L. Yang and Z. Zhang, *ACS Appl. Nano Mater.*, 2020, **3**, 8224–8231.

9  S. Singh, J. K. Vaishnav and T. K. Mukherjee, *ACS Appl. Nano Mater.*, 2020, **3**, 3604–3612.

10  T. Boobalan, M. Sethupathi, N. Sengottuvelan, P. Kumar, P. Balaji, B. Gulyás, P. Padmanabhan, S. T. Selvan and A. Arun, *ACS Appl. Nano Mater.*, 2020, **3**, 5910–5919.

11  M. Xiao, Z. Liu, N. Xu, L. Jiang, M. Yang and C. Yi, *ACS Sens.*, 2020, **5**, 870–878.

12  S. Yu, W. Li, Y. Fujii, T. Omura and H. Minami, *ACS Sustainable Chem. Eng.*, 2019, **7**, 19157–19166.

13  F. Arshad and M. P. Sk, *ACS Appl. Nano Mater.*, 2020, **3**, 3044–3049.

14  A. Sarkar, A. Chakraborty, T. Chakraborty, S. Purkait, D. Samanta, S. Maity and D. Das, *Inorg. Chem.*, 2020, **59**, 9014–9028.

15  K. P. Carter, A. M. Young and A. E. Palmer, *Chem. Rev.*, 2014, **114**, 4564–4601.

16  H. Xu, C. Zhu, Y. Chen, Y. Bai, Z. Han, S. Yao, Y. Jiao, H. Yuan, W. He and Z. Guo, *Chem. Sci.*, 2020, **11**, 11037–11041.

17  S. A. A. Razavi and A. Morsali, *Coord. Chem. Rev.*, 2020, **415**, 213299.

18  A. Nain, Y. T. Tseng, Y. S. Lin, S. C. Wei, R. P. Mandal, B. Unnikrishnan, C. C. Huang, F. G. Tseng and H. T. Chang, *Sens. Actuators, B*, 2020, **321**, 128539.

19  D. L. Ma, S. Y. Wong, T. S. Kang, H. P. Ng, Q. B. Han and C. H. Leung, *Methods*, 2019, **168**, 3–17.

20  Y. Guo, L. Zhang, S. Zhang, Y. Yang, X. Chen and M. Zhang, *Biosens. Bioelectron.*, 2015, **63**, 61–71.

21  Z. Zhang, Z. Wei, F. Meng, J. Su, D. Chen, Z. Guo and H. Xing, *Chem. - Eur. J.*, 2020, **26**, 1661–1667.

22  Z. Shaghaghi and R. Rezanezhad, *ChemistrySelect*, 2018, **3**, 5534–5540.

23  Z. Xu, L. Hu, J. Yuan, Y. Zhang, Y. Guo, Z. Jin, F. Long, Y. Long, H. Liang, S. Ruan and Y.-J. Zeng, *Adv. Mater. Interfaces*, 2020, **7**, 1902075.

24  D. Dai, J. Yang, Y. Wang and Y.-W. Yang, *Adv. Funct. Mater.*, 2021, **31**(1), 2006168.

25  R. Kumar, P. Gahlyan, N. Yadav, M. Bhandari, R. Kakkar, M. Dalela and A. K. Prasad, *Dyes Pigm.*, 2017, **147**, 420–428.

26  X. Wu, S. Zhang, Q. Niu and T. Li, *Tetrahedron Lett.*, 2016, **57**, 3407–3411.

27  J. Shi and Z. Zhang, *Inorg. Chim. Acta*, 2020, **511**, 119790.

28  R. Wei, Z. Wei, L. Sun, J. Z. Zhang, J. Liu, X. Ge and L. Shi, *ACS Appl. Mater. Interfaces*, 2016, **8**, 400–410.

29  A. Shylaja, S. R. Rubina, S. S. Roja and R. R. Kumar, *Dyes Pigm.*, 2020, **174**, 108062.

30  J. Gao, Y. He, Y. Chen, D. Song, Y. Zhang, F. Qi, Z. Guo and W. He, *Inorg. Chem.*, 2020, **59**, 10920–10927.

31  Q. Yan, W. Liu, H. Wen, X. Zhibin and Z. Meng, *ChemistrySelect*, 2020, **5**, 1878–1883.

32  P. Madhu, S. Ponnusamy and R. Sribalan, *New J. Chem.*, 2019, **43**, 11069–11081.

33  Y. e. Yu, Y. Wang, H. Yan, J. Lu, H. Liu, Y. Li, S. Wang, D. Li, J. Dou, L. Yang and Z. Zhou, *Inorg. Chem.*, 2020, **59**, 3828–3837.

34  B. X. Shen and Y. Qian, *ChemistrySelect*, 2017, **2**, 2406–2413.

35  R. S. Darole, D. B. Christopher Leslee, A. Mukherjee, R. G. Gonnade, S. Karuppannan and B. Senthilkumar, *Appl. Organomet. Chem.*, 2020, **34**, e5867.

36  Y. Zhang, Y. Feng, H. Guo, A. Abdurahman, X. Ai, Z. Zhang and M. Zhang, *Asian J. Org. Chem.*, 2020, **9**, 1081–1086.

37  K. Kaur, S. Chaudhary, S. Singh and S. K. Mehta, *Sens. Actuators, B*, 2016, **232**, 396–401.

38  P. S. Nayab and M. Shkir, *Sens. Actuators, B*, 2017, **251**, 951–957.

39  B. Zhao, T. Liu, Y. Fang, L. Wang, B. Song and Q. Deng, *Tetrahedron Lett.*, 2016, **57**, 4417–4423.

40  K. Thenmozhi and H. Jonnagaddala, *Mater. Chem. Front.*, 2020, **4**(5), 1471–1482.

41  A. Han, H. Su, G. Xu, M. Khan and H. Li, *RSC Adv.*, 2020, **10**, 23372–23378.

42  X. Zhu, Y. Duan, P. Li, H. Fan, T. Han and X. Huang, *Anal. Methods*, 2019, **11**, 642–647.

43  B. Li, J. Tian, D. Zhang and F. Tian, *Luminescence*, 2017, **32**, 1567–1573.

44  X. Xia, D. Zhang, C. Fan and S. Pu, *Appl. Organomet. Chem.*, 2020, **34**, e5841.

45  H. Fang, N. Wang, L. Xie, P. Huang, K. Y. Deng and F. Y. Wu, *Sens. Actuators, B*, 2019, **294**, 69–77.

46  X. He, W. Xiong, L. Zhang, C. Xu, J. Fan, Y. Qian, J. Wen, F. Ding and J. Shen, *Dyes Pigm.*, 2020, **174**, 108059.

47  L. Peng, Z. Zhou, X. Wang, R. Wei, K. Li, Y. Xiang and A. Tong, *Anal. Chim. Acta*, 2014, **829**, 54–59.

48  H. F. Xie, C. J. Yu, Y. L. Huang, H. Xu, Q. L. Zhang, X. H. Sun, X. Feng and C. Redshaw, *Mater. Chem. Front.*, 2020, **4**, 1500–1506.

49  S. K. Padhan, N. Murmu, S. Mahapatra, M. K. Dalai and S. N. Sahu, *Mater. Chem. Front.*, 2019, **3**, 2437–2447.

50  N. Dey, A. Ali, M. Kamra and S. Bhattacharya, *J. Mater. Chem. B*, 2019, **7**, 986–993.

51  S. N. Ansari, A. K. Saini, P. Kumari and S. M. Mobin, *Inorg. Chem. Front.*, 2019, **6**, 736–745.

52  S. Gharami, K. Aich, D. Sarkar, P. Ghosh, N. Murmu and T. K. Mondal, *New J. Chem.*, 2019, **43**, 1857–1863.

53  P. Karmakar, S. Manna, S. S. Ali, U. N. Guria, R. Sarkar, P. Datta, D. Mandal and A. K. Mahapatra, *New J. Chem.*, 2018, **42**, 76–84.

54  D. Y. Patil, A. A. Patil, N. B. Khadke and A. V. Borhade, *Inorg. Chim. Acta*, 2019, **492**, 167–176.

55  Q. Yu, X. Zhang, S. T. Wu, H. Chen, Q. L. Zhang, H. Xu, Y. L. Huang, B. X. Zhu and X. L. Ni, *Chem. Commun.*, 2020, **56**, 2304–2307.

56  A. Finelli, V. Chabert, N. Hérault, A. Crochet, C. Kim and K. M. Fromm, *Inorg. Chem.*, 2019, **58**, 13796–13806.

57  M. S. H. Faizi, S. Gupta, V. Mohan K, V. K. Jain and P. Sen, *Sens. Actuators, B*, 2016, **222**, 15–20.

58  S. Jena, P. Dhanalakshmi, G. Bano and P. Thilagar, *J. Phys. Chem. B*, 2020, **124**, 5393–5406.

59  G. Hu, H. Jia, Y. Hou, X. Han, L. Gan, J. Si, D. H. Cho, H. Zhang and J. Fang, *Anal. Chem.*, 2020, **92**, 4371–4378.

60  A. Podder, V. P. Murali, S. Deepika, A. Dhamija, S. Biswas, K. K. Maiti and S. Bhuniya, *Anal. Chem.*, 2020, **92**, 12356–12362.

61  A. M. Koorts and M. Viljoen, *Arch. Physiol. Biochem.*, 2007, **113**, 30–54.

62  W. Xu, T. Barrientos and N. C. Andrews, *Cell Metab.*, 2013, **17**, 319–328.

63  D. R. Richardson, D. J. R. Lane, E. M. Becker, M. L. H. Huang, M. Whitnall, Y. S. Rahmanto, A. D. Sheftel and P. Ponka, *Proc. Natl. Acad. Sci. U. S. A.*, 2010, **107**, 10775–10782.